Electronic Supplementary Material (ESI) for Nanoscale.

Supplementary information

Synthesis of Ni-Au-ZnO Ternary Magnetic Hybrid Nanocrystals with Enhanced Photocatalytic Activity

Deqian Zeng, Yuanzhi Chen,* Zhichao Wang, Junbao Wang, Qingshui Xie and Dong-Liang Peng*

Department of Materials Science and Engineering, College of Materials, Xiamen University, Xiamen 361005, People's Republic of China

Synthesis of ZnO nanocrystals.

In a typical synthesis, 0.55 mmol of $Zn(OAc)_2 \cdot 2H_2O$ was added into a mixed solution containing 10 mL of OAm and 4 mL of BA, and then the mixed solution was heated to 60 °C for 10 min. Finally the solution was heated up to 195 °C and kept at this temperature for 45 min before cooling down to room temperature naturally. After that, the generated products were washed by hexane, ethanol and acetone several times, separated from solution by centrifugation, and then dried in vacuum.

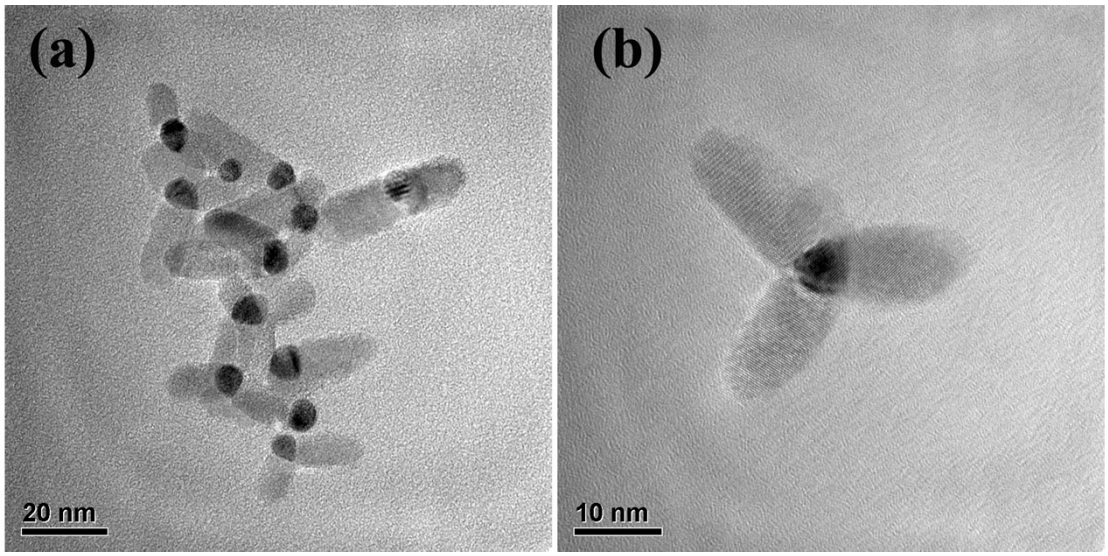

Fig. S1 TEM image (a) and HRTEM image (b) of Au-ZnO nanomultipods.

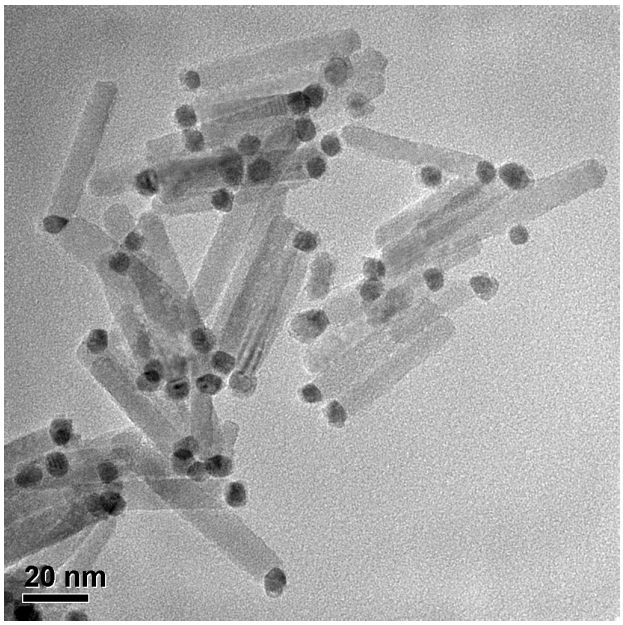

Fig. S2 TEM image of Au-ZnO nanorods.

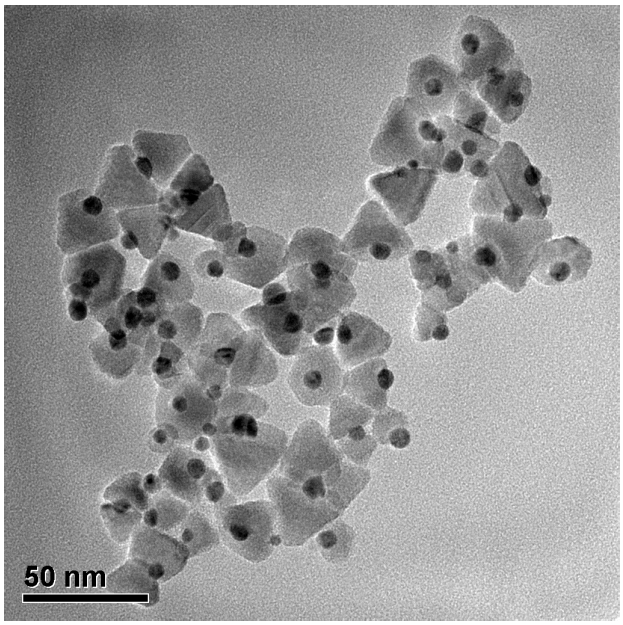

Fig. S3 TEM image of Au-ZnO nanopyramids.

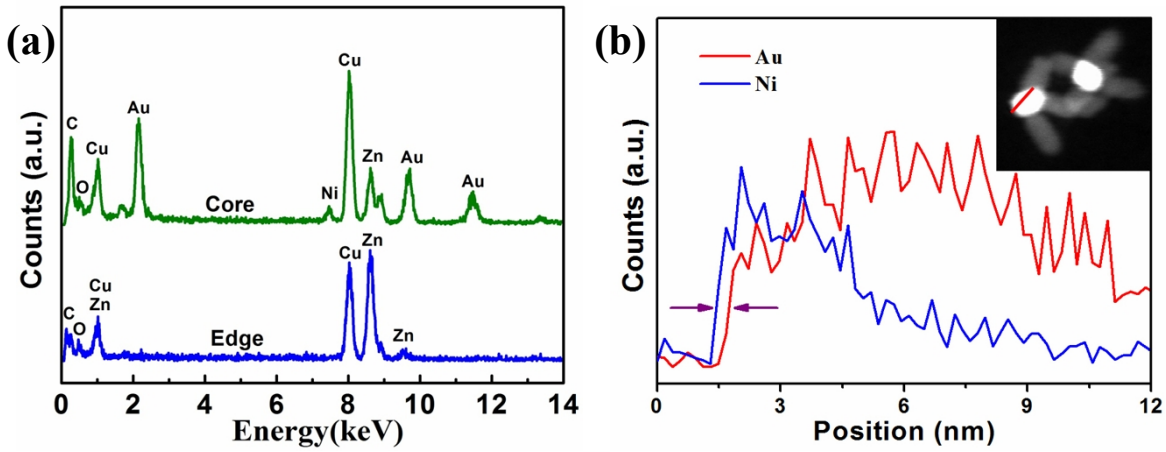

Fig. S4 (a) EDS spectra of Ni-Au-ZnO hybrid nanomultipods. (b) STEM-EDS line-scan analysis of an individual Ni-Au-ZnO hybrid nanomultipods shown in the upper inset.

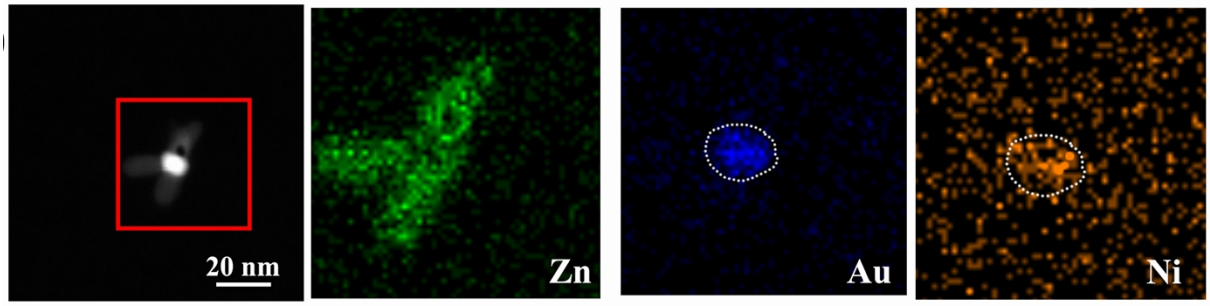

Fig. S5 HAADF image (left) and EDS elemental maps of Zn, Au and Ni of an individual Ni-Au-ZnO hybrid nanomultipods.

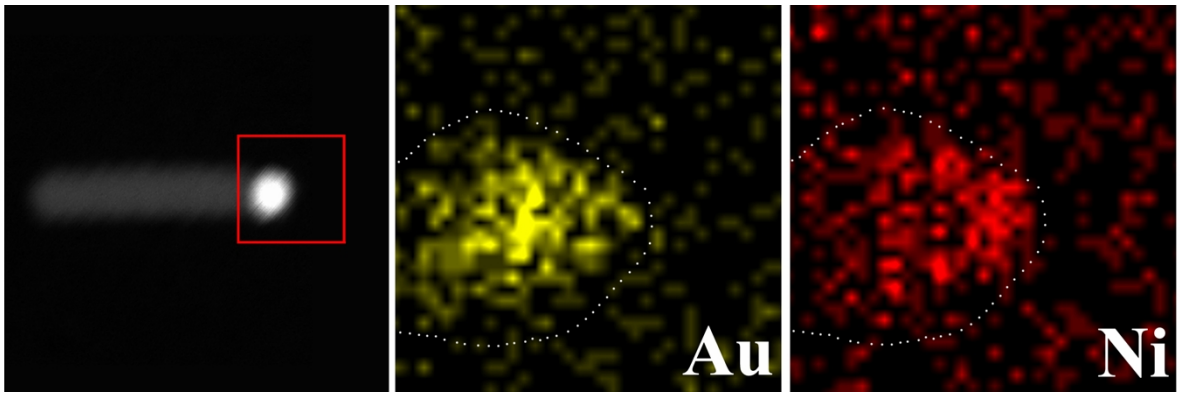

Fig. S6 HAADF image (left) and EDS elemental maps of Au and Ni of the metal portion taken from an individual Ni-Au-ZnO hybrid nanorod.

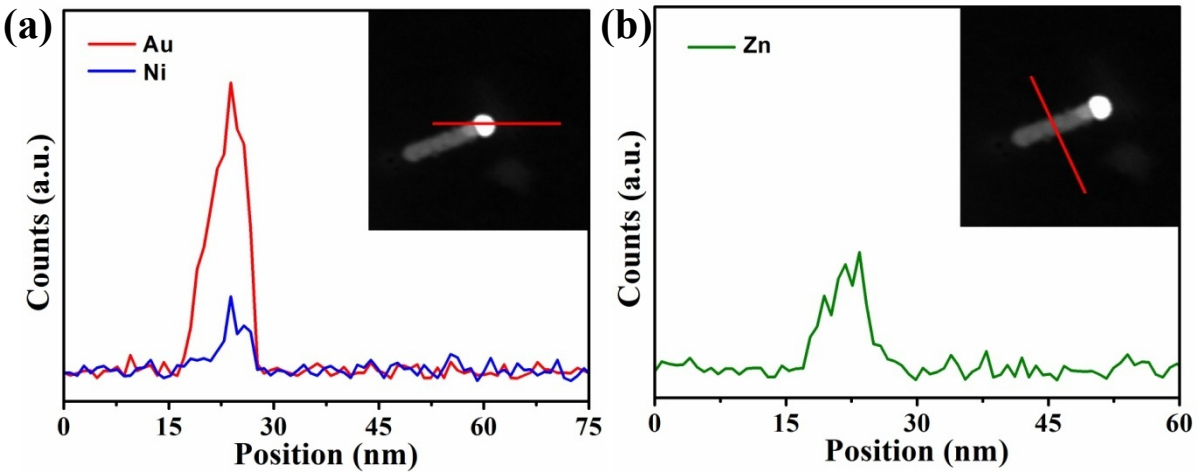

Fig. S7 STEM-EDS line-scan analysis of an individual Ni-Au-ZnO hybrid nanorod across the core (a) and rod (b) portions.

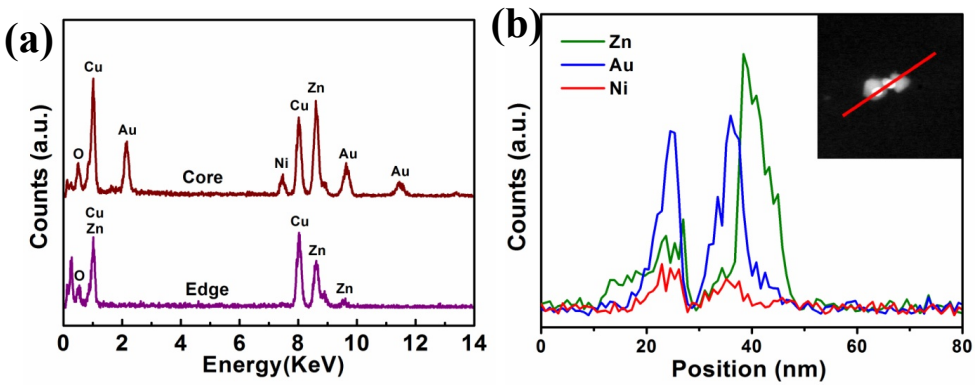

Fig. S8 (a) EDS spectra of an individual Ni-Au-ZnO hybrid nanopyramid. (b) STEM-EDS line-scan analysis of two Ni-Au-ZnO hybrid nanopyramids shown in the upper inset.

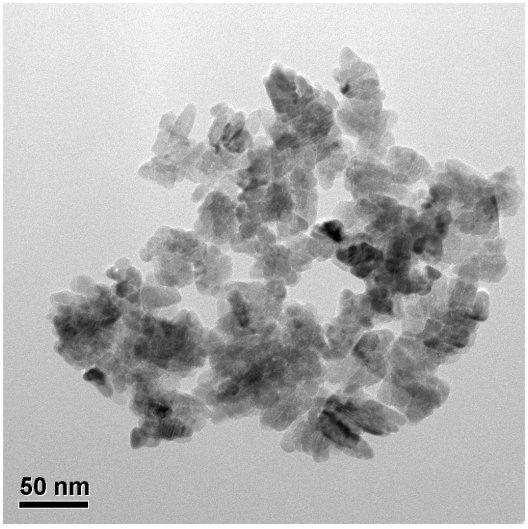

Fig. S9 TEM image of pure ZnO nanocrystals synthesized using the same method for preparing Ni-Au-ZnO hybrid nanorods except that no Au and Ni precursor were added.

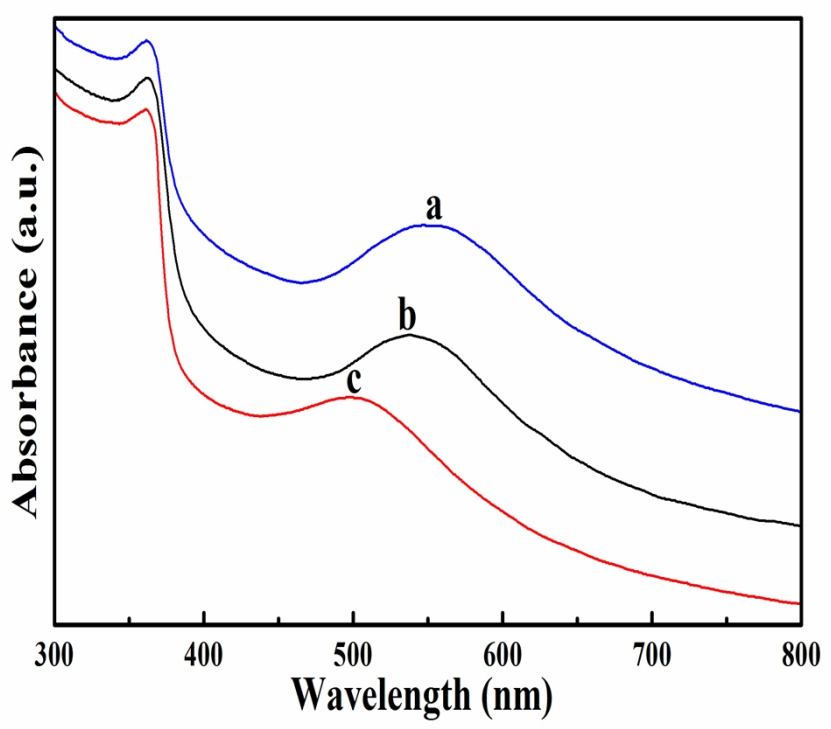

Fig. S10 UV-vis spectra of intermediate Au-ZnO hybrid nano-multipods (a), nanopyramids (b) and nanorods (c) before adding Ni.

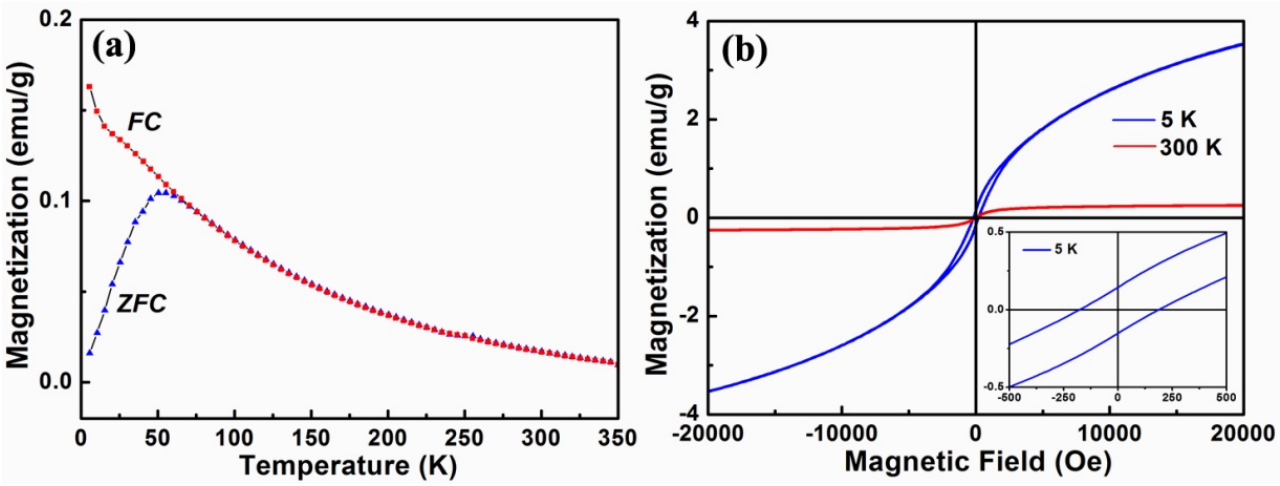

Fig. S11 ZFC-FC curves (a) in a measuring field and cooling field of 100 Oe, and magnetic hysteresis loops (b) of the Ni-Au-ZnO hybrid nanorods.

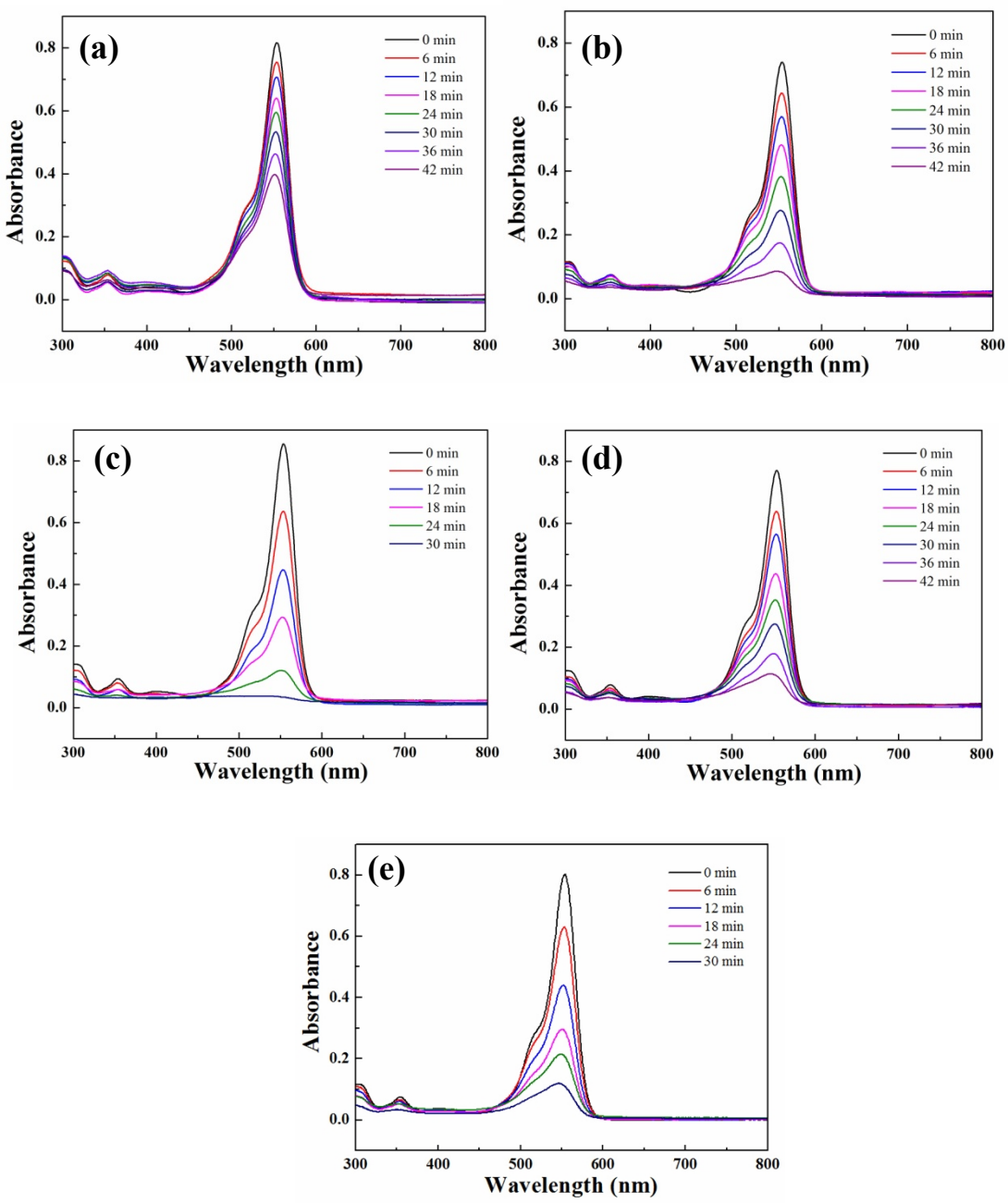

Fig. S12 Time-dependent UV-vis spectra recorded during the photocatalytic degradation of Rhodamine B by using pure ZnO nanocrystals (a), Ni-Au-ZnO hybrid nanomultipods (b), Ni-Au-ZnO hybrid nanorods (c), Ni-Au-ZnO hybrid nanopyramids (d), and Degussa P25 TiO_2 (e).

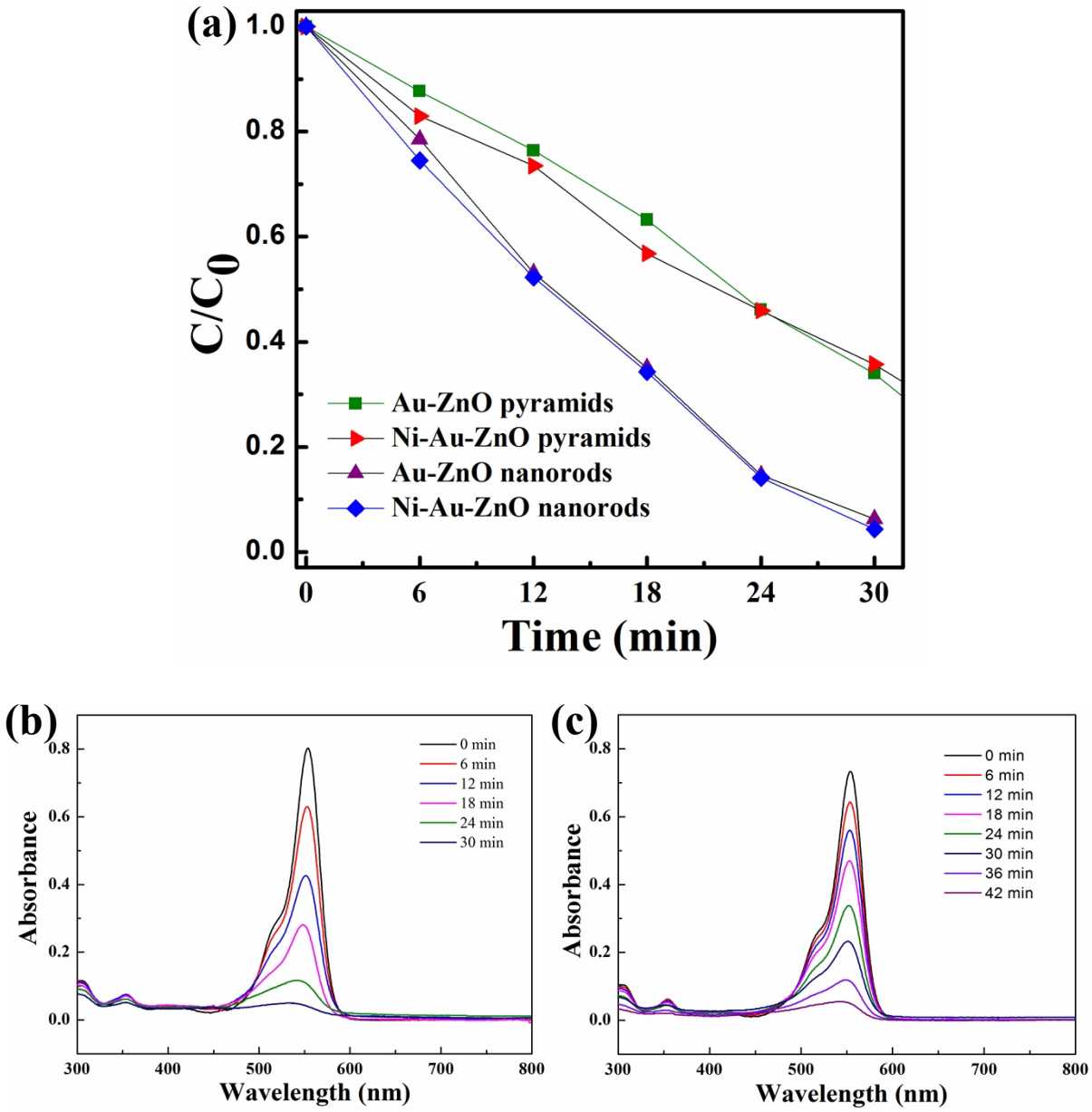

Fig. S13 (a) Time profiles of the photocatalytic degradation of RhB by different Au-ZnO and Ni-Au-ZnO samples under UV light irradiation. (b) and (c) are the time-dependent UV-vis spectra recorded during the photocatalytic degradation of Rhodamine B under UV light irradiation by using Au-ZnO hybrid nanorods and Au-ZnO nanopyramids, respectively.

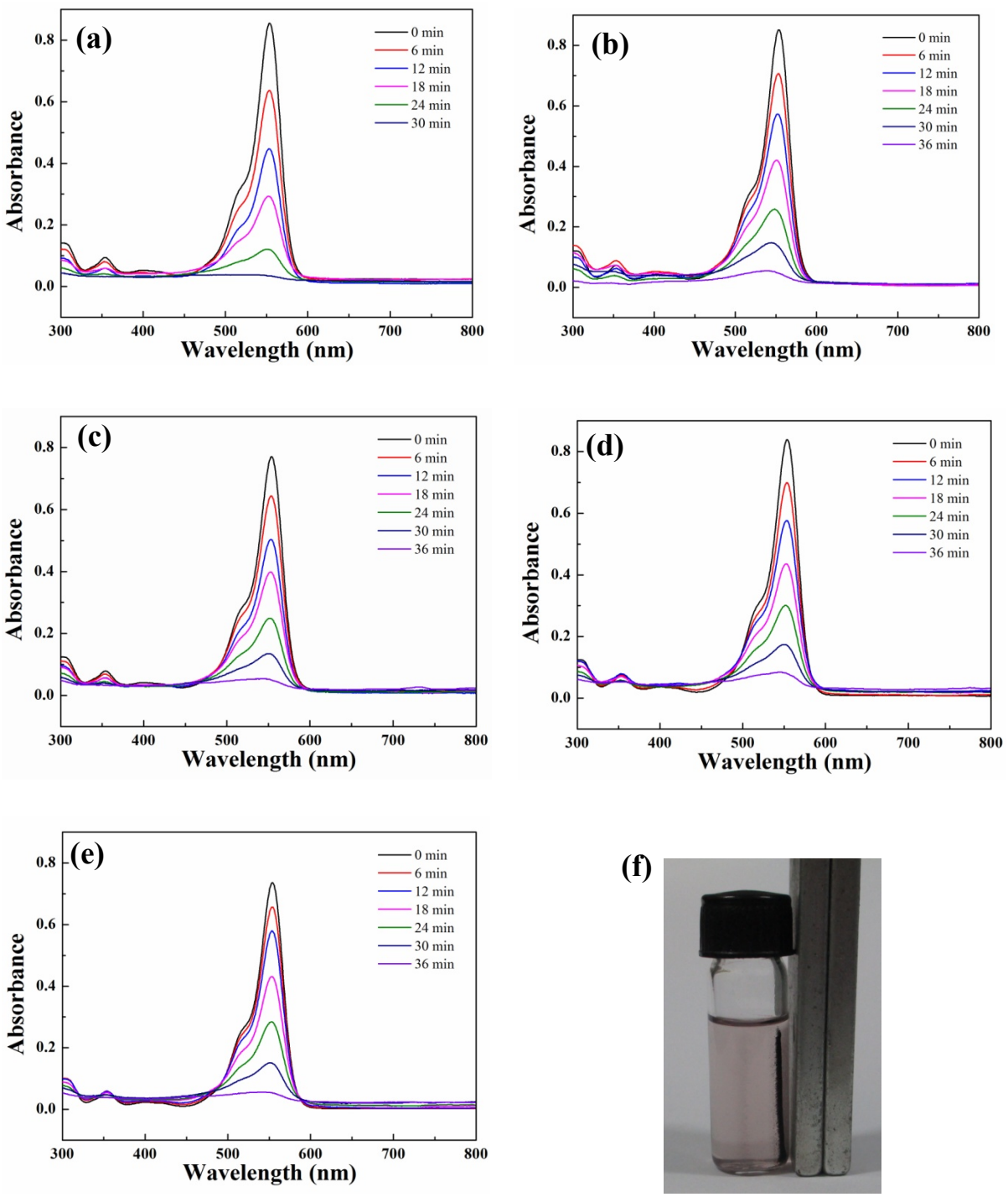

Fig. S14 (a), (b), (c), (d) and (e) are the time-dependent UV-vis spectra recorded during the photocatalytic degradation of Rhodamine B under UV light irradiation by using Ni-Au-ZnO hybrid nanorods for the 1st run, 2nd run, 3rd run, 4th run and 5th run, respectively. (f) The photographic image of Ni-Au-ZnO hybrid nanorods collected by using a magnet.

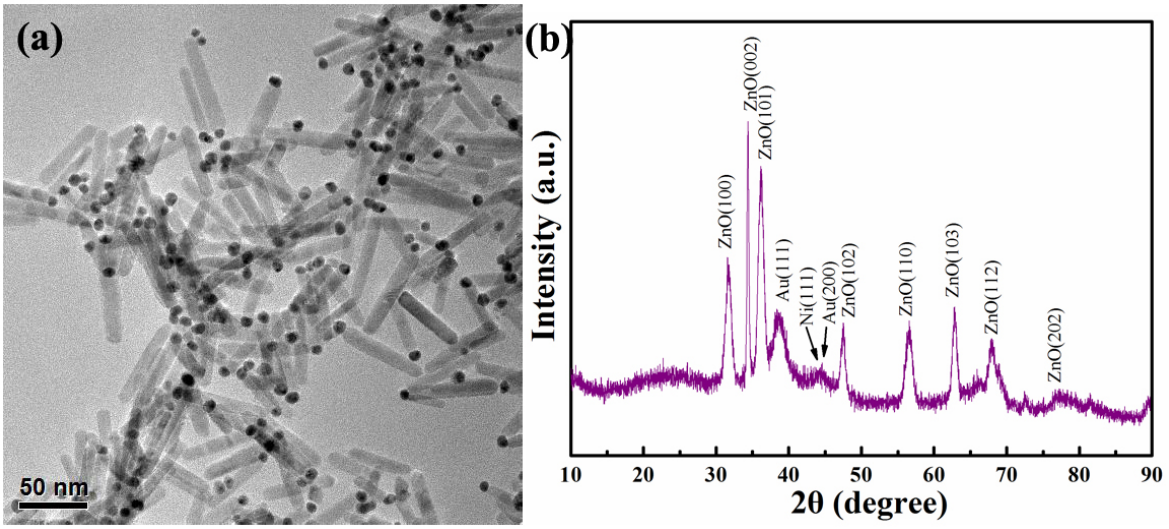

Fig. S15 TEM image (a) and XRD pattern (b) of Ni-Au-ZnO hybrid nanorods after cycled photocatalytic reactions.